Development of a Resonator with Automatic Tuning and Coupling Capability to Minimize Sample Motion Noise for *in Vivo* EPR Spectroscopy

Guanglong He, Sergey Petryakov, Alexandre Samouilov, Michael Chzhan, Periannan Kuppusamy, and Jay L. Zweier

EPR Center and Division of Cardiology, Department of Medicine, The Johns Hopkins University School of Medicine,
5501 Hopkins Bayview Circle, Baltimore, Maryland 21224

EPR spectroscopy has been applied to measure free radicals *in vivo*; however, respiratory, cardiac, and other movements of living animals are a major source of noise and spectral distortion. Sample motions result in changes in resonator frequency, *Q*, and coupling. These instabilities limit the applications that can be performed and the quality of data that can be obtained. Therefore, it is of great importance to develop resonators with automatic tuning and automatic coupling capability. We report the development of automatic tuning and automatic coupling provisions for a 750-MHz transversely oriented electric field reentrant resonator using two electronically tunable high *Q* hyperabrupt varactor diodes and feedback loops. In both moving phantoms and living mice, these automatic coupling control and automatic tuning control provisions resulted in an 8- to 10-fold increase in signal-to-noise ratio. © 2001 Academic Press

***Key Words*:** *in vivo* EPR; varactor diode; automatic tuning; automatic coupling; spin label.

INTRODUCTION

There has been a great need for the development of new resonators and techniques to enable the application of EPR spectro scopy for the measurement of free radicals and other paramagnetic centers in large biological samples and in living animals. A variety of lumped circuit devices have been developed for these applications over the past decade including loop–gap and reentrant resonators (*1–8*). These resonators, at L-band frequencies and below, along with a reflection bridge have made *in vivo* and *ex vivo* applications possible (*1–9*). Recently, we have reported the development of a reentrant resonator design with transverse oriented capacitive gap (TERR) with high *Q*, above 1500, wide frequency tuning range, and capacitive coupling (*9*). However, when measurements are performed on living animals, cardiac, respiratory, and other sample motions result in altered resonator frequency and *Q*, giving rise to instability and noise.

The conventional reflection microwave bridge utilizes an automatic frequency control (AFC) loop whereby the microwave oscillator is locked to the frequency of the EPR resonator. The AFC technique uses frequency modulation of the microwave oscillator and associated AFC signal detection and processing circuitry to automatically tune the frequency of the microwave oscillator to the frequency of the resonator. If there is a living animal in the resonator, the respiratory, cardiac, and muscular movements of the animals can cause changes of the resonant frequency of the resonator. The AFC circuit tracks this change, resulting in variation of the oscillator frequency, thus introducing distortion of the EPR spectrum with the magnitude of this distortion dependent on the amplitude of the frequency shift. The movements of the animal also change the impedance of the resonator, causing a mismatch of the resonator to the 50-Ω coaxial transmission line. This mismatch of the resonator results in altered reflected power to the bridge detector, in turn producing prominent noise spikes on the baseline of the spectrum. In some cases with large movement and small EPR signals, this motion-induced noise can be so large that the true EPR spectrum is completely obscured by the baseline noise, making EPR measurements impossible.

To address these problems, electronic tuning techniques were introduced for either automatic coupling control (ACC) (*10–12*) or, more recently, automatic frequency tuning control (ATC) (*8, 10*) using either varactor diodes or piezoelectric actuators. Each of these approaches has relative advantages and disadvantages.

A major difficulty of using a piezoelectric actuator to perform automatic tuning and automatic coupling is the limited acoustic isolation of the mechanical mode from any background mechanical noise. Another limitation is the relatively slow time response of the mechanical adjustment, as well as the difficulty of obtaining relatively large mechanical excursions of the actuator necessary at low frequencies. However, there are also some advantages to using a piezoelectric actuator. The piezoelectric actuator method is free from maximum RF power limitations. The piezoelectric actuator itself is also not directly affected by field modulation.

Varactor diodes, being free from the problems associated with mechanical noise, time response, and complexity of mechanical design, may be a preferable method for resonator control at low

frequencies (RF through S-band). However, the main problem limiting the application of varactor diodes for automatic tuning and automatic coupling is that the varactor diode placed within the modulated magnetic field rectifies the modulation signal and picks up a modulation-induced voltage. This causes the reverse-biasing voltage on the varactor to be altered by the modulation field. Thus, through this coupling a modulated signal will be added to the detection circuit, altering actual magnetic modulation amplitude and/or phase, finally resulting in EPR signal distortion and baseline offset. This modulation signal can mix with the EPR signal, making accurate measurements of the EPR signal impossible.

While successful approaches have been reported on given resonators for either ACC or ATC, there have been no prior reports of combined use of both ACC and ATC resonator provisions in order to enable *in vivo* whole body measurements of free radicals in small living animals such as mice or rats.

In order to solve these technical problems and implement automatic tuning and automatic coupling provisions for *in vivo* EPR measurements of small animals at 750 MHz, we developed a new TERR with a central solid brass stationary capacitive plate. To overcome the modulation pickup problem, two miniature high Q microwave varactor diodes were placed directly into wells machined in this brass plate and capped with circular metal capacitive discs to couple with the coupling and tuning plates of the resonator. Upon minimizing the physical dimensions of the varactor arrangement and shielding of the biasing leads inside the solid brass stationary capacitive plate, modulation pickup was virtually eliminated. Using appropriate ATC and ACC feedback loops, the performance of the resonator was tested on moving phantoms and living mice. The automatic coupling and automatic tuning provisions reduced the motion-induced noise by 8- to10-fold.

EXPERIMENTAL DESIGN AND SPECTROMETER SETUP

A. EPR Spectrometer System

A diagram of the spectrometer system used is shown in Fig. 1. It contains a 750-MHz microwave bridge, signal channel, the newly developed TERR resonator, the automatic tuning and automatic coupling feedback circuits, and customized computer software capable of performing spectral data acquisition (13–16). The automatic tuning feedback circuit contains the conventional AFC boosted by a voltage amplifier feeding the reverse-biased varactor tuning circuit. The automatic tuning feedback circuit contains the same phase detector as that used in the conventional AFC circuit, a voltage amplifier, and the reversely biased varactor tuning circuit. The automatic coupling circuit contains a lock-in amplifier, a mixer, a voltage amplifier, and the reversely biased varactor coupling circuit.

B. The 750-MHz Resonator Design

In order to accommodate the varactor diodes inside the resonator, a new resonator was built using copper-clad epoxy–glass
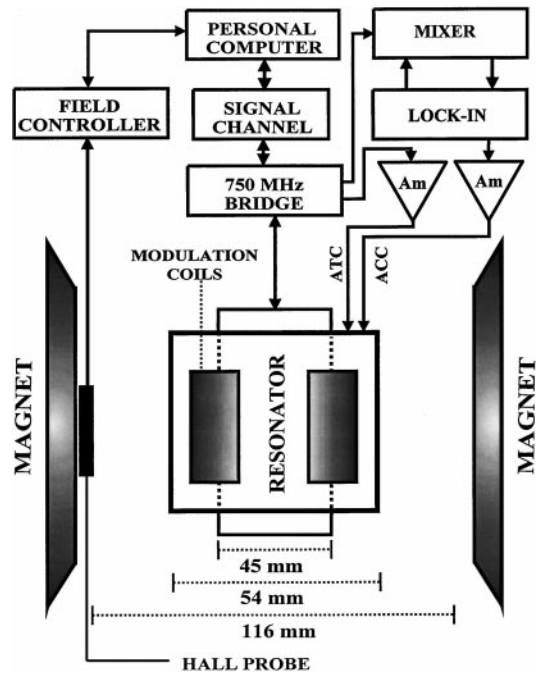

FIG. 1. Diagram of the 750-MHz spectrometer system. This includes the magnet, signal channel, field controller, custom-built 750-MHz microwave bridge (16), modified TERR resonator, and the automatic tuning and automatic coupling loops.

laminate material. Figure 2 shows the structure of the resonator and the setup for the two varactor diodes. The dimensions are shown in Table 1 and correspond to about a 10% reduction in size from the previously reported ceramic design (9). By introducing the varactor diodes into a TERR resonator, the resonant frequency will be shifted downward. In the worst case, the frequency of the resonator can be out of the range of the microwave bridge. We designed the new resonator with smaller size and higher resonant frequency, so that even after introduction of the varactor diodes and their downward shift of the resonant frequency, the resonator will still be able to work within the frequency range of our narrow band bridge (750 to 780 MHz).

The downward shift of the resonant frequency occurs due to capacitive loading by static capacitances of varactor diodes (see

TABLE 1
Specifications of the TERR Resonator

Parameter	Value
Overall dimensions outside (mm) (L × W × H)	162 × 54 × 140
Dimensions inside (mm) (L × W × H)	135 × 45 × 108
Center opening (mm)	45
Center frequency (MHz)	800
Center frequency (calculated) (MHz)	850
Center frequency setting range (MHz)	100−900
Center frequency tuning range (MHz)	±50
Unloaded Q without sample	2300
Unloaded Q with 30-g mouse	450
Maximum aqueous volume coupling capacity (ml)	50
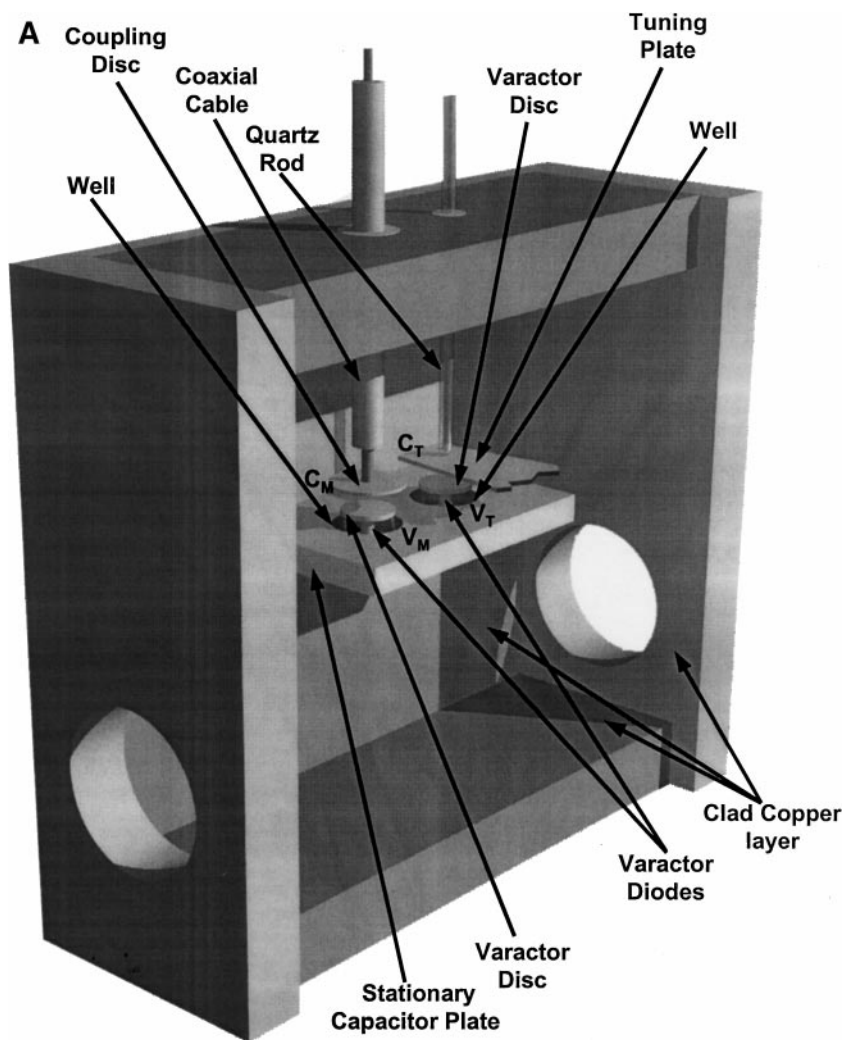
FIG. 2. Diagram and photograph showing the structure of the 750-MHz resonator with two varactor diode circuits inserted into the stationary capacitor plate. (A) In this diagram, the capacitance between the coupling disc and the stationary capacitor plate is labeled as C_M, the capacitance between the tuning plate and the stationary capacitor plate is labeled as C_T, and the automatic coupling and automatic tuning varactor diodes are V_M and V_T, respectively. The two diodes were mounted in two wells machined into the stationary capacitor plate to achieve direct coupling of the microwave power and better shielding from the modulation magnetic field. (B) Photograph of the 750-MHz resonator showing the resonator structure and the mounting of the 100-kHz field modulation coils on the outer surface of the sample holder.

detailed description in Section E). C_M is the mechanically adjustable capacitance between the coupling disc and the stationary capacitor plate, C_T is also the adjustable capacitance between the tuning plate and the stationary capacitor plate, and V_M and V_T are the tuning and coupling varactor diodes, respectively. The resonant frequency of the resonator is 800 MHz and the mechanical frequency tuning range is about 100 MHz (800 ± 50 MHz) without apparent degradation of the unloaded Q value of 2300. The unloaded Q with a 30-g mouse is 450 and the maximum aqueous volume coupling capacity is 50 ml without dropping the resonant frequency below 750 MHz, that is the low end of our narrow band bridge (750 to 780 MHz).

The resonator was constructed from copper-clad epoxy–glass laminate board (Copper-Clad G-10/FR4 Garolite from McMaster) instead of ceramic material to facilitate easy machining

and mechanical modifications. This composite material provides good thermal stability and acoustic dampening. Copperclad laminate board of 2-mm thickness was epoxy glued to a supporting laminate board of 10-mm thickness and cured at room temperature for 24 h. The thickness of the clad copper is about 50 μm. These boards were machined into six pieces to form the resonator box of dimensions shown in Table 1. Then a 5-mm width of silver strip foil (50-μm thickness) was glued with conductive silver epoxy to cover each edge of the copper-clad boards. The clad boards were then put into an oven at 170°C for 6 h. In the final step, the clad boards were silver-plated and tightly assembled. In this way, the microwave leakage was minimized. This plus the precise mechanical machining and careful alignment of the boards and the stationary capacitor plate (shown in Fig. 2) were very crucial for obtaining the maximum Q value.
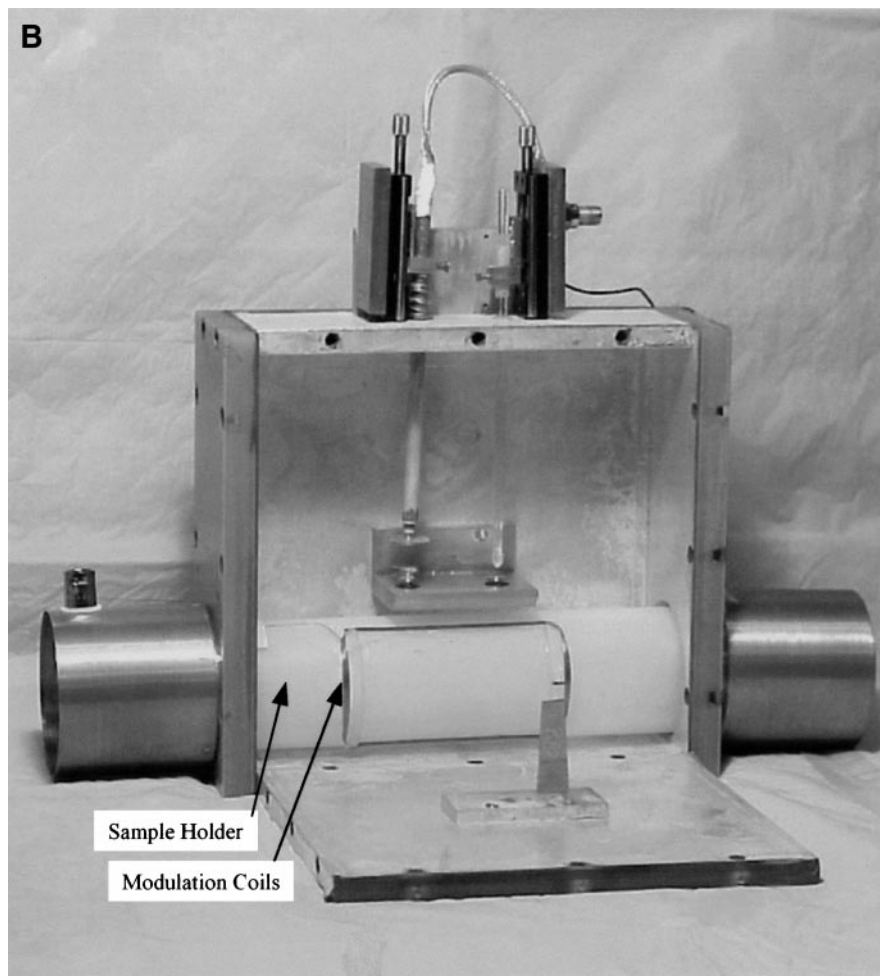
FIG. 2—*Continued*

In view of this, to enhance the magnitude of the modulation field in the sample area, a set of cylindrical saddle modulation coils mounted on the surface of a rexolyte tubular support were placed inside the resonator (shown in Fig. 2B). The stationary plate of the resonator capacitor element was machined out of solid brass and silver-plated. Two cylindrical wells were machined in the body of this plate to house the two varactor diodes and the biasing circuits. These wells were positioned on the same axis as the corresponding tuning and coupling capacitive plates. Efficient shielding of the varactor diodes and biasing leads from coupling to the magnetic field modulation was achieved by embedding the varactor diodes into the wells of the solid brass capacitor plate. The varactor diodes in the wells were capped by silver-plated brass discs (labeled varactor discs in Fig. 2) to enable coupling to the corresponding tuning and coupling plates and further complete the shielding from modulation pickup.

As shown in Fig. 2, the resonator structure contains two reentrant inductive loops of square cross section. The capacitive area of the resonator is formed by two plates protruding into the center of the resonator from the opposing sidewalls. These two plates,

the tuning plate and the stationary capacitor plates, are shown in Fig. 2A. A sample holder was placed into the lower loop and the coupling disc was placed in the upper loop, as shown in Fig. 2B. The plane of the capacitive gap is transverse to that in the conventional reentrant resonator.

A brief comparison of the new resonator with the previously reported ceramic TERR resonator (*9*) shows that the dimension of the new resonator is scaled down 10% and this resulted in a 50-MHz increase in the resonator frequency. Since the sample arm is smaller and more compact, the filling factor is higher and there is a greater effect of a given size lossy sample on Q. It also follows that the maximum aqueous volume coupling capacity is smaller.

C. Mechanical Design for Automatic Coupling Varactor Diode Placement

Figure 3A shows the setup of the automatic coupling varactor diode (high Q hyperabrupt tuning varactor, MA4ST553, M/A-COM Inc.) inside the brass stationary capacitor plate.
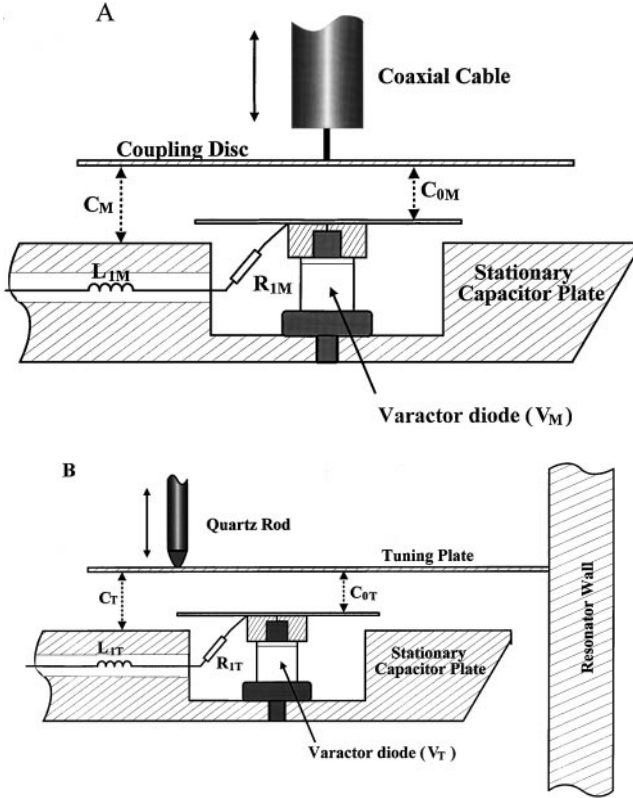
FIG. 3. Mechanical layout of the stationary capacitor plate with the varactor diode circuits for the automatic coupling (A) and automatic tuning (B) loops. R_{1M} is the Q depressing resistor for the coupling circuit. L_{1M} is the choke inductance. The varactor diode was capped with a small brass disc (varactor disc). This metal disc formed a small capacitor C_{0M} between the disc and the coupling disc, in series with the capacitance of the varactor, and its value served to adjust the variable coupling range achieved on voltage biasing of the varactor. R_{1T} is the Q depressing resistor for the tuning circuit. L_{1T} is the choke inductance. The tuning varactor diode was also capped with a small brass disc (varactor disc) forming a capacitor C_{0T} between this disc and the tuning plate, in series with the varactor. Its value served to adjust the variable tuning range achieved on voltage biasing of the varactor.

The total capacitance of the varactor at -4 V is between 1.08 and 1.32 pF. When biased with a DC voltage from -0.7 to -20 V, the capacitance of the varactor changes from 1.8 to 0.45 pF with good linearity. According to manufacturer's specifications, the Q value of the varactor at -4 V bias voltage at 50 MHz is approximately 500. Underneath the coupling disc (C_M) and inside the metal stationary plate, a well of 5-mm diameter was machined. The coupling varactor diode was mounted in the well and thus grounded. The varactor diode was capped with a brass disc of 5.5-mm diameter using conductive epoxy compound. This metal disc formed a small capacitor (the capacitance between this varactor disc and the coupling disc is C_{0M}), which is in series with the capacitance of the varactor. A small diameter well was machined in the body of the stationary plate to provide shielded housing for the biasing leads and circuitry.

D. Mechanical Design for the Automatic Tuning Varactor Diode Placement

Figure 3B shows the placement of the automatic tuning varactor diode inside the stationary capacitor plate, which is analogous to the coupling varactor placement. Underneath and on the axis of the tuning pate (C_T), another well of 5-mm diameter was machined and the tuning varactor diode was placed into it. On top of the varactor a 5.5-mm-diameter brass disc was attached with silver epoxy glue to form another small capacitor (the capacitance between this varactor disc and the tuning plate is C_{0T}). A small diameter well machined in the body of the plate housed the biasing circuitry.
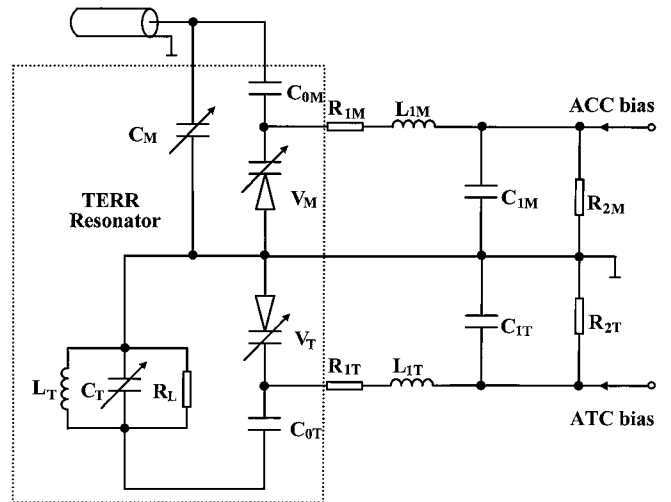
E. Equivalent Circuit of the Resonator with Automatic Coupling and Automatic Tuning Varactor Diodes

Figure 4 shows the equivalent circuit of the resonator and the related circuits for the automatic tuning and automatic coupling varactor diodes. Capacitors C_M and C_T, inductance L_T, and sample load R_L form the lumped circuit equivalent of the resonator. Without the varactor circuit, the coupling and tuning capacitance are C_M and C_T, respectively. With the varactor circuit connected, the coupling capacitance of the resonator is changed to C, which is given as

$$C = C_M + \frac{C_{0M}C_{VM}}{C_{0M} + C_{VM}},$$

where

$$C_{VM} = \frac{C_0}{(1 + V/\phi)^\gamma} + \frac{\phi^\gamma C_0}{(\phi + V)^\gamma}.$$

FIG. 4. The equivalent circuit for the resonator with the automatic coupling and tuning provisions. The input ports for the introduction of the ACC and ATC bias potentials to the two diodes are shown on the right. C_{1M} and C_{1T} are shunting capacitors. C_M, C_T, L_T, and R_L are lumped circuit equivalents of the resonator. R_{2M} and R_{2T} are control circuit input resistors.

C_{VM} is the capacitance of the varactor with a reverse-biasing DC potential across the diode junction. C_0 is the zero-bias capacitance of the varactor. V is the voltage across the diode junction. ϕ is the contact potential of the junction of the varactor diode and is equal to 0.5 V. γ is the power law of the junction and is determined by the impurity gradient. For step junction including hyperabrupt junction, it is equal to 0.5. The capacitance for the tuning circuit is described by a similar expression. The microwave power is introduced into the resonator by the coupling capacitor C_M and by changing this capacitance the resonator can be coupled to the 50-Ω transmission line either in the presence or in the absence of a lossy biological sample. By changing C_T, the frequency of the resonator can be tuned within a 100-MHz range. By changing the reverse-bias DC voltage on the two varactor diodes, the capacitance of the coupling and tuning capacitors can be readily changed. By carefully adjusting the size of the capacitors C_{0M} and C_{0T} (changing the diameters of the discs capping the varactors), an adequate electronic tuning and coupling range can be achieved. DC voltage bias to the varactor diodes is introduced through R_{2M} and R_{2T}, respectively. L_{1M} and L_{1T} are two choke inductors. C_{1M} and C_{1T} form low-pass filters with the above-mentioned chokes. It is practically important to connect these resistors directly to the varactor diode leads. Otherwise the choke inductances may form relatively high Q resonant modes with the varactor diodes, which may compete with the main resonance. To suppress this self-resonant mode, a relatively large resistor of 15 kΩ is connected with very short leads to the varactors of both the tuning and the coupling circuits. By carefully adjusting the value of the C_{0M} and C_{0T} (diameters of the discs), we were able to achieve the required tuning and coupling ranges. The tuning range of the tuning varactor diode circuit is about ±5 MHz with a DC potential swing of 15 V. The coupling varactor diode provided about 3 dB of coupling adjustment with the resonator loaded by a lossy sample. In order to verify the coupling and tuning capacity of the varactor diodes, we measured the coupling and tuning change caused by the movement of a 30-g anesthetized mouse inside the resonator using a network analyzer (HP 8720). The range of the change of the coupling was less than 1 dB. The range of the change of the tuning was less than 1 MHz. These changes were within the coupling and tuning capability of the varactor diode.

F. Automatic Tuning Feedback Circuit

Figure 5A shows the feedback circuit for the automatic tuning. When the switch K is in position 1, the circuit works as an AFC feedback circuit. The DC bias voltage from the AFC phase detector is connected to the oscillator and tunes the frequency of the oscillator to the frequency of the resonator. When the switch is in position 2, the oscillator tuning port is maintained at a constant DC voltage (7.8 V). The DC bias voltage is taken from the AFC phase detector and connected to a voltage amplifier and then from the output of the amplifier to the tuning varactor diode V_T. In this case, the signal from the AFC phase detector

is used to adjust the resonance frequency of the resonator to the frequency of the oscillator. If the phasing is correct, the feedback circuit will lock the frequency of the resonator to the frequency of the oscillator automatically. Thus the resonance frequency of the resonator is fixed even in the presence of sample motion.

G. Automatic Coupling Feedback Loop

Figure 5B shows the automatic matching feedback loop for the varactor diode V_M. The reference signal at a frequency of 20 kHz is supplied from an SRS-850 lock-in amplifier (Stanford Research) to the mixer in order to modulate the incoming DC voltage corresponding to the detector diode current. This voltage is obtained from the RF bridge preamplifier. The 20-kHz modulated signal is fed back to the lock-in amplifier. The lock-in amplifier performs detection, filtering, phase adjustment, and amplification of the feedback signal. After scaling in the voltage amplifier, this conditioned signal is supplied to the coupling control varactor diode V_M. A switch in the voltage amplifier provides an easy way to change the phase of the output signal by 180°.

Automatic tuning feedback circuit

Automatic coupling feedback loop
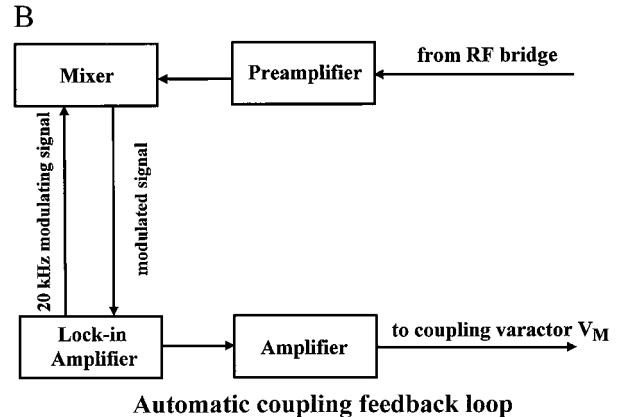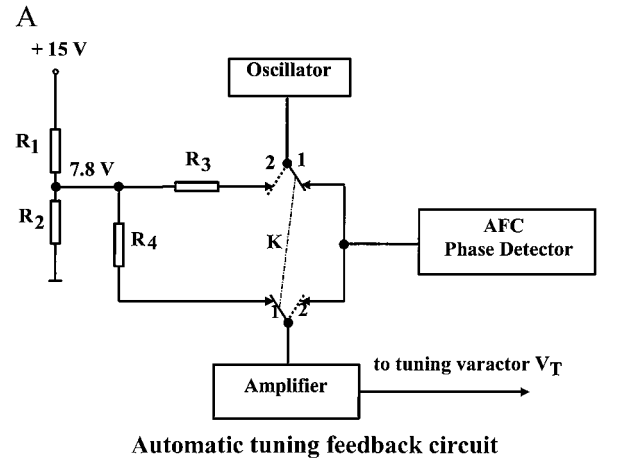
FIG. 5. (A). ATC feedback circuit. The circuit maintains constant bias voltages to the oscillator and to the voltage amplifier. R_1 and R_2 are 13 and 15 kΩ, respectively. R_3 and R_4 are both 10 kΩ. (B). ACC feedback loop. The reference signal from the lock-in amplifier is 20 kHz.
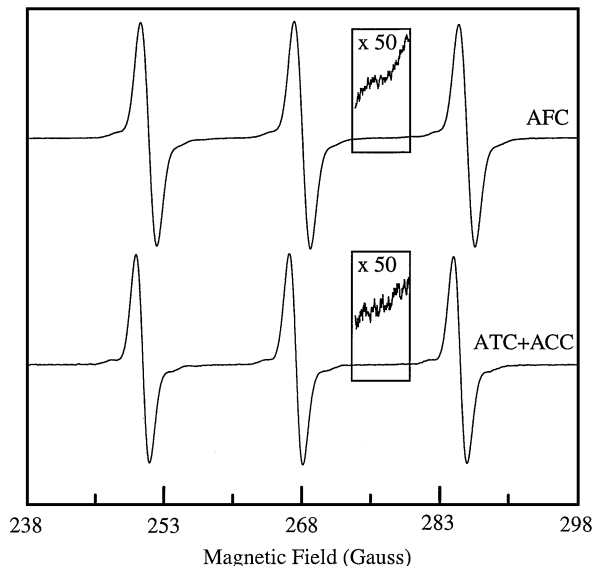
FIG. 6. The spectra of 30 ml of 1 mM TEMPO in water with AFC and with ATC plus ACC. The EPR parameters for both spectra are as follows: microwave frequency 750-MHz, microwave power 30 mW, time constant 40 ms, acquisition time 15 s. The parameters for the ATC and ACC circuits are as follows: the voltage on the tuning varactor diode is 7.8 V, the voltage on the coupling varactor diode is 11.0 V, the gain of the lock-in amplifier is 20 dB, the frequency of the reference signal is 20 kHz, the amplitude of the reference signal is 0.5 V.

This switch, together with the continuous phase adjustment capability of the lock-in amplifier, enables correct loop phasing.

## EXPERIMENTAL APPLICATIONS AND RESULTS

A. Application to a Moving Phantom

It was expected that some additional noise might be introduced into the signal with the incorporation of the two control loops into the system. In order to measure this factor, we performed EPR measurements on a stationary phantom, consisting of a bottle filled with 30 ml of aqueous 1 mM 2,2,6,6-tetramethylpiperidinoxyl radical (TEMPO). The spectra for both the conventional configuration (with AFC) and with introduction of ATC plus ACC are shown in Fig. 6. The two insets (noise signal shown scaled up by a factor of 50) illustrate that the noise in the presence of the ATC and ACC loops is modestly increased by less than a factor of 2 compared to that with the standard bridge AFC.

In order to test the dynamic performance of the ATC and ACC system with a moving sample, a special actuator was built. The phantom with aqueous TEMPO solution was mounted to the end of a quartz rod, which provided the actuator movement from an 8-W audio speaker (15). Signals of variable frequency and amplitude from a function generator (Wavetek, Arbitrary Waveform
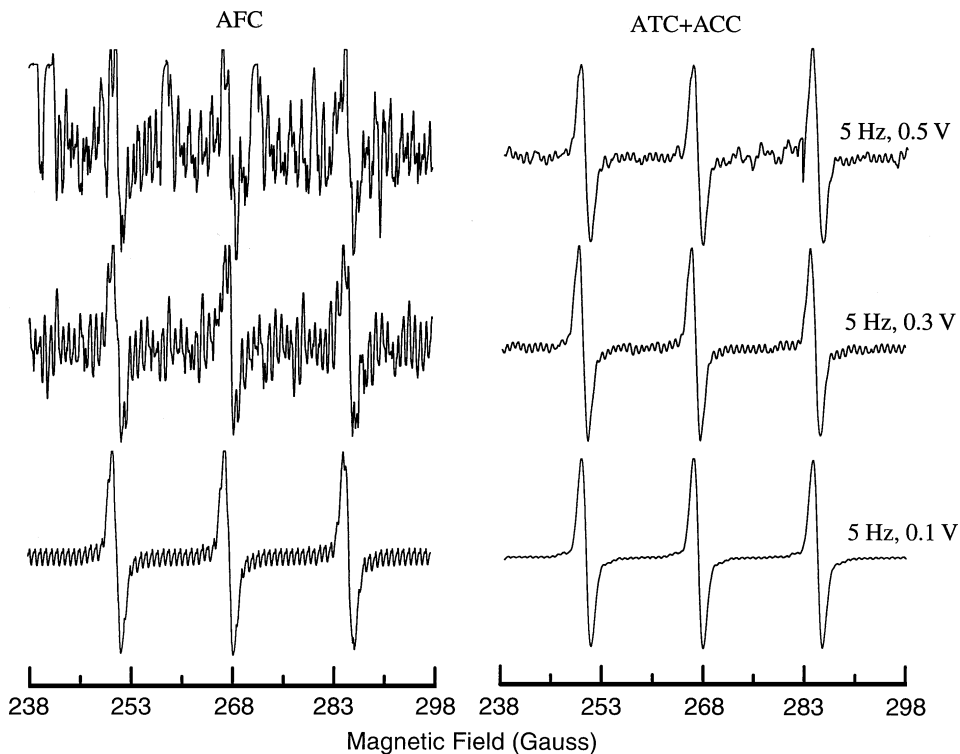
FIG. 7. Spectra of the moving 30 ml of 1 mM TEMPO sample with AFC (left scans) or ATC + ACC loops (right scans). The movement frequency is 5 Hz with each row showing variable excursion (0.1-V output from a function generator corresponds to 1-mm excursion and the response is linear up to 1 V). Acquisition parameters and parameters for the automatic tuning and automatic coupling circuits are the same as in Fig. 6.
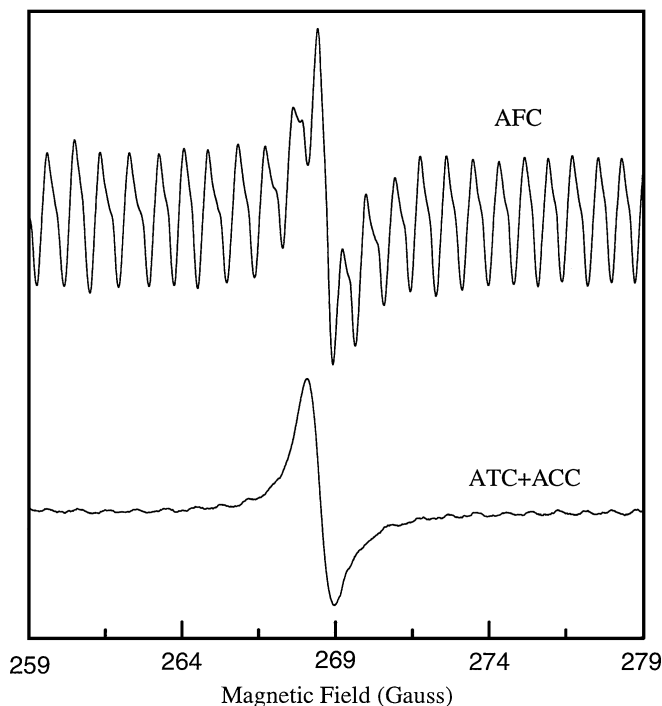
FIG. 8. Spectra of charcoal in a living mouse with AFC (top) or with ATC plus ACC (bottom). The mouse was fed the charcoal spin probe the day prior to the measurements. Acquisition parameters are same as those in Fig. 6.

Generator Model No. 75) were used to control the frequency and excursion magnitude of sample motion to simulate the motions of a living object.

Before EPR measurement, we measured the frequency change, the Q value change, and the coupling change of the moving phantom with a network analyzer. With a movement of 5-mm excursion, the frequency changed 1.5 MHz and the Q changed 1.3%; with a movement of 3-mm excursion, the frequency changed 1 MHz and the Q changed 0.67%; with a movement of 1-mm excursion, the frequency changed 0.5 MHz and the Q changed 0.59%. Within 5-mm excursion movement, the coupling change is less than 2.5 dB. Figure 7 shows the spectra obtained in conventional AFC mode, as well as with the ATC and ACC system using the TEMPO phantom at 5 Hz frequency of movement for different excursions controlled by the driving voltage to the speaker. Comparison of the spectra obtained with AFC and with ATC and ACC shows a signal-to-noise ratio improvement of about 8 times. It was observed that the ATC and ACC loops could remarkably compensate for most of the noise introduced by the moving phantom.

B. Application to Living Mice

After evaluation and validation on the moving phantom, we applied the automatic tuning and automatic coupling techniques to the living mouse. C3H mice weighing 30 to 40 g were used (*16*). Commercially obtained charcoal was used as the spin label.

Before the mice were fed with charcoal, solid-food intake was stopped for 12 h, after which the mice were fed a mixture of charcoal and sugar for 24 h. The mice then were lightly anesthetized with 10 mg/kg pentobarbital by intraperitoneal injection. During anesthesia the animals' respiratory rate and heart rate remained stable. The respiratory rate was about 80/min and the heart rate was about 400/min. Figure 8 shows the spectra from a mouse using either AFC or ATC and ACC loops. At least 10-fold improvement in the signal-to-noise ratio is seen with the use of the ATC/ACC system compared to that obtained with conventional AFC.

DISCUSSION AND CONCLUSIONS

Sample motion-derived noise has been a major factor limiting the extension of EPR spectroscopy for the measurement and imaging of free radicals in living animals. Sample motions induce changes in resonator frequency, Q, and resultant coupling, all of which greatly perturb the measured spectrum using conventional CW EPR instrumentation. We recently reported the development of a reentrant resonator design with a transverse oriented capacitive plate that enables wide-range frequency tuning and efficient capacitive coupling (*9*). This resonator has enabled whole body EPR spectroscopy and imaging of mice at 750 MHz. While EPR measurements on living animals are possible with this and other resonators, the quality and signal-to-noise ratio in these measurements are greatly limited by respiratory motion and other animal movements.

With the varactor diode-based automatic tuning and automatic coupling system described, we achieved a large improvement in signal-to-noise ratio in the EPR spectra of both moving phantoms and living animals. In general, an 8- to 10-fold improvement in signal-to-noise ratio was seen compared to that with standard AFC. Moving phantom experiments demonstrated that the feedback circuits compensate motional noise very well at 5 Hz or lower motional frequencies. As would be expected with the fast response characteristics of varactor diodes, the response time of the circuit is not limited by the varactor response. At higher frequencies, above 10 Hz, the quenching of the noise was less effective. This limitation is not due to the time response of the varactor diode but arises from the time constant of the AFC circuit that is used in our automatic tuning loop. Since the rates of the typical respiratory and cardiac movements are less than 1 or 7 Hz, respectively, the loop response time was adequate for compensating the movements of small animals, including mice and rats.

With the good shielding from the magnetic field modulation provided by the placement of the varactors inside the brass body of the stationary capacitor plate of the resonator, the observed influence of the 100-kHz field modulation on the diodes was negligible, and there was no apparent modulation pickup-induced perturbation on the EPR signal or the signal baseline level.

One of the limitations for the use of varactor diodes, directly coupled to the microwave field of the resonator, is that they start

working nonlinearly with respect to this field at high incident power. In other words, at high power levels the varactor diode actually acts as a detector diode so that a microwave-induced DC voltage appears across the junction. In order to determine the practical microwave power range for the application of varactor diodes, an oscilloscope was connected across the junction of the varactor diodes. Then the microwave power was increased gradually. Up to 40 mW of microwave power there was no recognizable voltage rectified by the varactor diodes. When the microwave power was increased to 50 mW, a −2-V voltage was observed and the performance of the ATC and ACC began to be degraded. The maximum microwave power that we could use in our design was about 40 mW, which is sufficient for a range of *in vivo* applications.

Varactor diodes have been previously used for either automatic tuning or coupling in *in vivo* EPR measurements. Over a decade ago, Halpern *et al.* (*11*) reported the development of an automatic coupling control technique for a lumped component resonator at 250 MHz. More recently, Hirata *et al.* (*10*) developed a surface coil resonator at L-band with automatic tuning and coupling control for localized EPR spectroscopy of living animals. However, there have been no prior reports of a resonator design suitable for whole body EPR measurements in small animals capable of both automatic coupling control and automatic tuning control.

Our goal was to develop a resonator suitable for whole body EPR spectroscopy and imaging in living mice. We also used varactor diodes to achieve electronic tuning and coupling; however, there are some fundamental differences in our resonator design and approach compared to that of the prior reports. First, we used a high Q TERR cavity resonator. As previously reported, this resonator has the advantage that it is mechanically tunable over a broad frequency range (*9*) and has a high unloaded Q, Q_u of 2300. Even when loaded with a lossy biological sample such as a 30-g mouse, the Q_u remains relatively high with a value of 450. Since the Q is high, this can enable higher sensitivity; however, movements of the animal impose higher level noise. Therefore, to realize the potential sensitivity enhancements of the TERR design, the use of ATC and ACC techniques is of particular importance. Second, the positioning of the varactor diodes within the resonator is a unique innovation with two major advantages. The first advantage is that the distortion from the 100-kHz field modulation is greatly reduced because the varactor diodes are placed into a well in the center of the brass stationary capacitive plate and this provided good shielding. The other advantage is that, since the varactor diodes are placed directly within the resonator, this enables the coupling varactor to be directly adjacent to the capacitive coupling plate and the tuning varactor to be directly adjacent to the tuning plate, providing efficient use of the varactor diodes to tune and couple the resonator. With this TERR resonator design utilizing ATC and ACC techniques, we achieved an 8- to 10-fold improvement of signal-to-noise ratio on moving phantom samples and living mice.

In conclusion, a highly effective automatic tuning and automatic coupling system was developed for a 750-MHz transversely oriented electric field resonator using two electronically tunable high Q hyperabrupt varactor diodes and feedback loops. This system enabled a 10-fold increase in signal-to-noise ratio for EPR measurements in small living animals such as mice. This development should greatly facilitate the performance of *in vivo* and *ex vivo* EPR spectroscopy and imaging of free radicals and paramagnetic probes in small living animals as well as in isolated perfused organs such as the heart and lungs.

REFERENCES

1. W. Froncisz and J. S. Hyde, The loop–gap resonator: A new microwave lumped circuit ESR sample structure, *J. Magn. Reson.* **47**, 515–521 (1982).

2. J. S. Hyde and W. Froncisz, loop–gap resonators, *Electron Spin Reson.* **10A**, 175–184 (1986).

3. R. Diodato, M. Alecci, J. A. Brivati, and A. Sotgiu, Resonant inductive coupling of RF EPR resonators in the presence of electrically conducting samples, *Meas. Sci. Technol.* **9**(5), 832–837 (1998).

4. R. Diodato, M. Alecci, J. A. Brivati, V. Varoli, and A. Sotgiu, An optimization of axial RF field distribution in low-frequency EPR loop-gap resonators, *Phys. Med. Biol.* **44**(5), N69–N75 (1999).

5. G. A. Rinard, R. W. Quine, B. T. Ghim, S. S. Eaton, and G. R. Eaton, Easily tunable crossed-loop (bimodal) EPR resonator, *J. Magn. Reson. A* **122**(1), 50–57 (1996).

6. W. Piasecki, W. Froncisz, and W. L. Hubbell, A rectangular loop–gap resonator for EPR studies of aqueous samples, *J. Magn. Reson.* **134**(1), 36–43 (1998).

7. M. Chzhan, M. Shteynbuk, P. Kuppusamy, and J. L. Zweier, An optimized L-band ceramic resonator for EPR imaging of biological samples, *J. Magn. Reson. A* **105**(1), 49–53 (1993).

8. M. Chzhan, P. Kuppusamy, and J. L. Zweier, Development of an electronically tunable L-band resonator for EPR spectroscopy and imaging of biological samples, *J. Magn. Reson. B* **108**(1), 67–72 (1995).

9. M. Chzhan, P. Kuppusamy, A. Samouilov, G. L. He, and J. L. Zweier, A tunable reentrant resonator with transverse orientation of electric field for *in vivo* EPR spectroscopy, *J. Magn. Reson.* **137**(2), 373–378 (1999).

10. H. Hirata, T. Walczak, and H. M. Swartz, Electronically tunable surface-coil-type resonator for L-band EPR spectroscopy, *J. Magn. Reson.* **142**(1), 159–167 (2000).

11. H. J. Halpern, D. P. Spencer, and J. Polen, Imaging radio frequency electron-spin-resonance spectrometer with high resolution and sensitivity for *in vivo* measurements, *Rev. Sci. Instrum.* **60**(6), (1989).

12. S. McCallum and F. Resmer, Automatic coupling control system for radio frequency in vivo electron paramagnetic resonance based on a piezoelectric controlled capacitor, *Rev. Sci. Instrum.* **70**(12), 4706–4710 (1999).

13. J. L. Zweier and P. Kuppusamy, Electron paramagnetic resonance measurements of free radicals in the intact beating heart: A technique for detection

and characterization of free radicals in whole biological tissues, *Proc. Natl. Acad. Sci. USA* **85**, 5703–5707 (1988).

14. P. Kuppusamy, M. Chzhan, A. Samouilov, P. Wang, and J. L. Zweier, Mapping the spin density and lineshape distribution of free radicals using 4D spectral-spatial EPR imaging, *J. Magn. Reson. B* **107**, 116–125 (1995).

15. P. Kuppusamy, M. Chzhan, P. H. Wang, and J. L. Zweier, Three-dimensional gated EPR imaging of the beating heart: Time-resolved measurements of free radical distribution during the cardiac contractile cycle, *Magn. Reson. Med.* **35**(3), 323–328 (1996).

16. G. L. He, R. A. Shankar, M. Chzhan, A. Samouilov, P. Kuppusamy, and J. L. Zweier, Noninvasive measurement of anatomic structure and intraluminal oxygenation in the gastrointestinal tract of living mice with spatial and spectral EPR imaging, *Proc. Natl. Acad. Sci. USA* **96**, 4586–4591 (1999).